New Generation Radiation-Grafted PVDF-*g*-VBC based Dual-Fiber Electrospun Anion Exchange Membranes*

*Ahmet Can Kırlıoğlu[a], Naeimeh Rajabalizadeh Mojarrad[a], Selmiye Alkan Gürsel[a,b], Enver Güler[c], Begüm Yarar Kaplan[b]**

[a] Sabanci University, Faculty of Engineering and Natural Sciences, 34956, Istanbul, Turkey

[b] Sabanci University, SUNUM Nanotechnology Research Center, 34956, Istanbul, Turkey

[c] Atılım University, Department of Chemical Engineering, 06830 Ankara, Turkey

***Corresponding author email:** begumyarar@sabanciuniv.edu

Abstract

Anion Exchange Membranes (AEM) have the potential to solve the cost issues of fuel cell technologies due to their basic environment that can allow the use of cheaper components. However, there is still a need to develop an ideal inexpensive, mechanically robust AEM with high ionic conductivity and ion exchange capacity (IEC). In this work, we present various dual-fiber electrospun membranes based on a novel radiation-grafted copolymer. First, the synthesis route of radiation-induced grafting of vinyl benzyl chloride (VBC) onto poly(vinylidene fluoride) (PVDF) to prepare PVDF-*g*-VBC was optimized. Then, PVDF-*g*-VBC powders were used to fabricate dual-fiber electrospun mats with inert PVDF and commercial Fumion-FAA-3 ionomer. Dual-fiber electrospun mats were hot-pressed and then quaternized with trimethylamine. Finally, mechanical properties, ion exchange capacity, ionic conductivity, and morphology of these prepared dual-fiber electrospun membranes were investigated. The dual-fiber membrane prepared with PVDF-*g*-VBC (88% of the total weight of the membrane) and PVDF: Fumion-FAA-3 (1:2) mix (12 wt%) realized ionic conductivity of 4.67 mS/cm at 25 ^{o}C, high ion exchange capacity of 1.35 mmol/g with Young's Modulus of 761 MPa. The membrane based on the combination of radiation grafting and dual-fiber electrospinning was prepared for the first time in literature and offers the prospect of tuning and fine-control of mechanical and physicochemical properties of AEMs.

Keywords: Dual-fiber electrospinning; Radiation-induced grafting; Anion exchange membrane; Fuel cells

1. Introduction

The need for better green energy technologies is of key importance due to the global climate change crisis mainly driven by the greenhouse effect of excessive CO_2 in the atmosphere [1]. Switching from fossil fuels to sustainable and renewable energy sources is an accentuated solution for decreasing CO_2 emissions globally [1]. The fuel cell technologies are well-studied

*Published by International Journal of Hydrogen Energy, doi: https://doi.org/10.1016/j.ijhydene.2023.05.345

greener alternatives to fossil fuel-based energy systems due to their higher efficiency, lower pollution, and more compact design. Proton Exchange Membrane Fuel Cells (PEMFCs) are the most common type of fuel cells that are commercially available over the years. However, their widespread commercialization as a cost effective energy conversion system is hindered because of certain cost and other technical issues. These include the usage of expensive Nafion® membranes as electrolyte, corrosion of various components due to their acidic medium, high fuel crossover [2]. Furthermore, the main reason for the high cost of PEMFCs is the use of rare earth catalysts, specifically, Pt group metals (PGM), which make up more than half of the fuel cell stack cost [3]. While the use of PGM catalysts is almost a necessity in the acidic environment of PEMFCs, the basic environment of AEMFCs provides a wider range of catalyst options including non-Pt-group elements such as Fe, Co [4–6].

Although anion exchange membrane fuel cells (AEMFCs) have many advantages over PEMFCs, the bottleneck of the AEMFCs' development is a promising anion exchange membrane (AEM) [7]. Therefore, AEMFC research is generally focused on developing an ideal membrane that can boost the advancement of AEMFC technologies, similar to the discovery of Nafion® boosted the PEMFC technologies. An ideal membrane for AEMFCs must have high hydroxide ionic conductivity, excellent chemical, dimensional, and mechanical stability to compete with PEMFCs in the market [8]. Hence, two main problems of AEM membranes need to be solved: i) low hydroxide ionic conductivity, and ii) inadequate chemical stability against alkaline attack at high temperatures. The main reason for the low ionic conductivity of AEMs is that OH^- ion is larger than the H^+ which hinders the mobility.[8] Another reason for the lower conductivity of AEMs than the PEMs can be attributed to the lack of microphase separation between hydrophilic and hydrophobic phases, which causes ion clustering and channels that allow ion transport in PEMs [9,10].

For the above-mentioned reasons, various AEM structures were developed by scientists, and the most noteworthy of them are AEMs synthesized via radiation-induced grafting [6,11,12]. Radiation-induced grafting is generally preferred in these studies due to the fact that other chloromethylation reactions of polymers require chloromethyl ether, which is a potent carcinogen and toxic material [13]. In these studies, the syntheses are carried out by directly irradiating the polymer film with a high-energy radiation source (^{60}Co or e-beam) to create radicals grafted with a monomer that can be functionalized to create pathways to conduct OH^- ions. In the literature, there is a fair amount of research on radiation-induced grafting of polymer films such as polyethylene or poly(ethene-*co*-tetrafluoroethene) [6,11,12]. Varcoe et al. extensively investigated the properties of the radiation-induced grafted membranes using ETFE or polyethylene as base films and VBC as grafted side chains [14]. They claimed that these membranes can be considered promising alternative for AEMFCs due to their high IEC (> 2 mmol/g) as well as superior ionic conductivity (> 200 mS/cm) in comparison with previous AEM membranes [14]. However, this grafting approach of the polymer films has several problems. First, the difficulty of monomer diffusion into the bulk of the film, therefore, the grafting generally takes place on the surface of the polymer film which is called “grafting front mechanism” [15]. Second, the lack of homogeneous grafting due to the geometric deformation of films during the process [16,17]. One of the solutions to overcome these problems is using irradiated powder polymers instead of pre-formed films as

*Published by International Journal of Hydrogen Energy, doi:
https://doi.org/10.1016/j.ijhydene.2023.05.345

the base polymer. Hence, we conducted the polymer synthesis by irradiating and grafting VBC onto PVDF in powder form which is the first time in the literature.

These irradiated powder polymers are needed to be made into compact films to be used in fuel cells because a porous structure of membrane would lead to fuel crossovers [18]. The electrospinning technique is selected to create polymer mats that can be hot-pressed into compact films. In the literature, film casting from solution and melt pressing methods are the most common techniques to prepare compact films from powder polymers [19,20]. Electrospinning is a versatile, simple, cost-effective technique commonly used to produce micro/nano-sized polymer fibrous materials for various applications such as membranes for fuel cells [21]. The produced fibrous mats via this technique can be easily converted to highly dense membranes via hot-pressing, which has several advantages over conventional film casting or melt-pressing methods. In electrospun membranes, the continuous fibrous structure with well-distributed functional groups gives rise to highly connected ion transfer sites for high ionic conduction [22]. This technique has been successfully applied in many different studies on composite fuel cell membranes. It has been reported that it provides various superior properties based on its use in fuel cells, particularly emphasizing its interaction at the nanoscale [18,23–25]. In these studies, it has been shown that proton exchange membranes exhibit better ionic conductivity, lower swelling in aqueous environments, and improved mechanical properties compared to membranes cast in film form by electrospinning. For example, Pintauro et al. fabricated dual-electrospun anion-exchange composite polysulfone-based membranes for the first time in literature [26]. These membranes showed 2.47 mmol/g IEC and 400 mS/cm ionic conductivity. However, the researchers did not include any fuel cell data regarding the performance of these membranes [27]. In these works, the electrospinning technique is used to control swelling by wrapping the charged polymer with the inert polymer.

Despite these advantages, studies on electrospun AEMs are quite limited. Park et al. produced dual-fiber mats using polyphenyl sulfone (PPSU) and chloromethylated polysulfone (CMPSF) (neutral/inert polymer matrix) for this purpose [28]. Here, the PPSU polymer was integrated as an inert polymer to control the swelling of the membrane in aqueous environments and to increase its mechanical strength. Another advantage is that the membrane's brittle structure in dry environments is transformed into a flexible membrane structure. They subsequently obtained AEMs through quaternization and alkalization of the mats [29]. Although the membranes exhibited high ionic conductivity and good mechanical properties, they showed significant swelling in aqueous environments (over 200%). Therefore, the same group cross-linked the mats they obtained by using aliphatic diol and diamine in their other two studies [28,30]. As a result of these studies, it was reported that increasing the crosslinking degree (from 4% to 7%) decreases the water uptake (from 250% to 140%). Although the membranes produced in these studies exhibited high ion exchange capacity and high ionic conductivity values, they were not tested in fuel cells, and their fuel performances were not demonstrated. This is most likely due to the anticipated easy deterioration of these membranes in fuel cell applications due to their high water uptake.

In order to combine the advantages of these two methods, in the present study, firstly we synthesized a novel PVDF grafted vinyl benzyl chloride copolymer (PVDF-*g*-VBC) by employing

*Published by International Journal of Hydrogen Energy, doi:
https://doi.org/10.1016/j.ijhydene.2023.05.345

^{60}Co irradiation to create active sites on poly(vinylidene fluoride) (PVDF) powder and grafting them with vinyl benzyl chloride (VBC) monomers. Then, this copolymer in powder form, along with inert PVDF and commercial Fumion ionomers is used to create dual-fiber (drawn from two distinct solutions simultaneously) electrospun mats with various dual-fiber ratios. The electrospun mats were then aminated and ion-exchanged to convert them into AEMs. Then, dual-fiber-based membranes were investigated in terms of their mechanical properties, ionic exchange capacity, ionic conductivity, and morphology. For the first time in the literature, dual-fiber electrospinning is utilized in combination with the radiation-grafted synthesis of PVDF-*g*-VBC to prepare novel membranes for AEMFC applications.

2. Material and methods

2.1. Materials

Polyvinylidene fluoride (PVDF) (SoleF®, M_w=380,000 g/mol) powders were acquired from Solvay, Belgium. N,N-dimethylacetamide (DMAc, 99%), 1-octyl-2-pyrrolidone (98%), VBC (97%, mixture of 2, 3- and 4-isomers), Tetrahydrofuran (THF), Trimethylamine solution (TMA, 45%), KOH, Toluene (≥99.5) were acquired from Sigma Aldrich, USA. Shredded Fumion-FAA-3 films are bought from Fumatech, Germany.

2.2. Grafting of poly(vinylidene fluoride) with vinyl benzyl chloride

First, PVDF powders are irradiated with γ-rays at Gamma-Pak Sterilization (Çerkezköy, Turkey) employing a ^{60}Co source. They are irradiated at room temperature with 50 kGy, then stored at -80 ^{o}C until the grafting reaction. Secondly, the grafting of PVDF is performed by mixing irradiated PVDF powder, vinyl benzyl chloride monomer (a mixture of 3- and 4-isomers) (Fig. 1.), and the surfactant 1-octyl-2-pyrrolidone (1%) in different solvents with various volumetric ratios listed in Table 1. This solution was degassed with N_2 for the specified periods in Table 1 before the reaction. Then, the reaction was initiated in a sealed two-necked round-bottom flask, using the various temperature, reaction times, and mixing speed parameters (Table 1). The synthesis setup is shown in Fig 2. After the reaction, the solution was filtered with a vacuum filter and washed three times with toluene to get rid of the homopolymer (PVBC) [19]. The degree of grafting is calculated by the following equation:

$$DoG[\%] = \frac{w_g - w_i}{w_i} \, x \, 100 \qquad (1)$$

Where w_g is the weight of the grafted polymer, w_i is the initial weight of the base polymer.

The highest degree of grafting was obtained with route 9 in which the copolymer is synthesized with a 50% monomer ratio in 49% IPA at 60 ^{o}C for 72 hours. The same parameters of route 9 are used to prepare another batch of PVDF-*g*-VBC but with an irradiation dose of 25 kGy. Route 9, with irradiation doses of 25 kGY and 50 kGy, is used for the rest of the experiments.

*Published by International Journal of Hydrogen Energy, doi:
https://doi.org/10.1016/j.ijhydene.2023.05.345

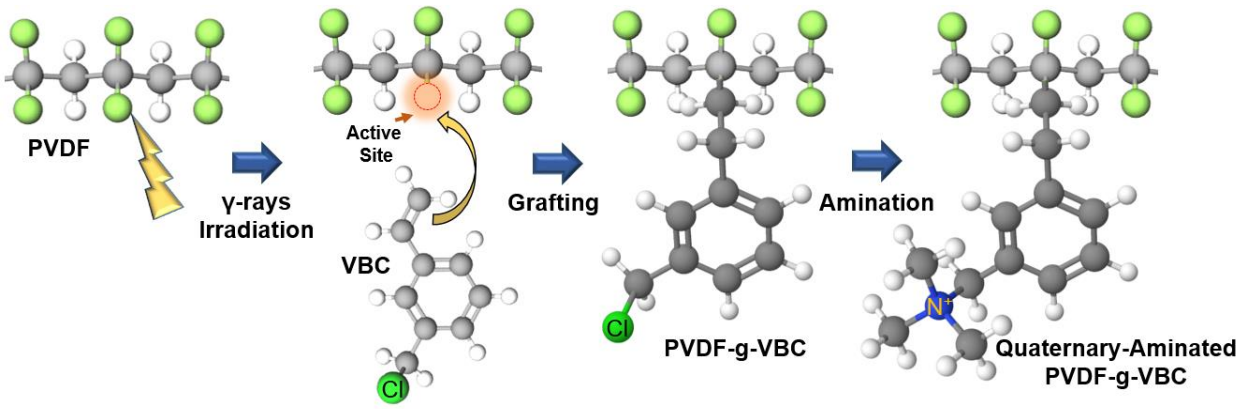

Figure 1. Outline of the PVDF-*g*-VBC-based anion exchange membrane production process. The steps are in the order of irradiation of the PVDF, grafting of VBC monomer into active sites, functionalization of the PVDF-*g*-VBC with TMA.

Table 1. Optimization of synthesis parameters and degree of grafting (%)

Synthesis Route	Solvent Content [v%]	Monomer Content [v%]	Irradiation dose [kGy]	Reaction Temperature [ºC]	Reaction Duration [h]	N_2 Purge Duration [h]	Degree of Grafting [%]
1	IPA 79%	VBC 20%	50	60	72	1	-
2	IPA 79%	VBC 20%	50	60	72	1	-
3	IPA 49%	VBC 50%	50	60	72	1	-
4	IPA 49%	VBC 50%	50	60	72	1	-
5	IPA:H_2O (1:1) 49%	VBC 50%	50	60	72	1	3
6	IPA:H_2O(1:1) 49%	VBC 50%	50	60	72	1	5
7	IPA:H_2O (4:1) 49%	VBC 50%	50	60	72	1	3

*Published by International Journal of Hydrogen Energy, doi: https://doi.org/10.1016/j.ijhydene.2023.05.345

8	IPA:H_2O (2:1) 49%	VBC 50%	50	60	72	1	6
9	IPA 49%	VBC 50%	50	60	72	3	15
10	IPA:H_2O (3:1) 49%	VBC 50%	50	60	72	3	9
11	IPA 49%	VBC 50%	50	70	72	3	10
12	IPA 49%	VBC 50%	50	60	72	3	11
13	IPA 49%	VBC 50%	50	60	96	3	12
14	IPA 49%	VBC 50%	25	60	72	3	9

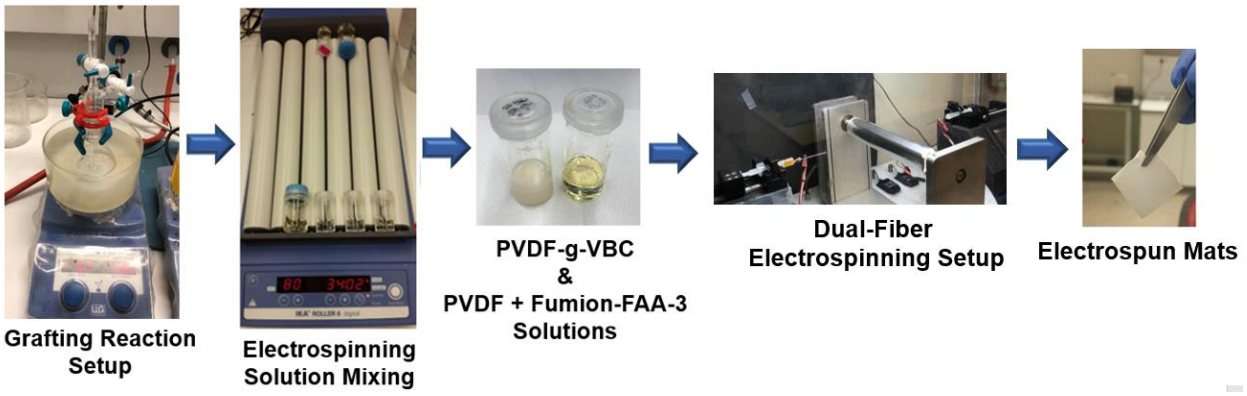

Figure 2. Preparation steps of the dual-fiber electrospun mats. The steps are in the order of grafting reaction of VBC onto PVDF powders, preparation of electrospinning solution with these powders, preparation of mats by dual-fiber electrospinning.

2.3 Characterization of PVDF-*g*-VBC powders

Obtained PVDF-*g*-VBC powders are characterized by Fourier transform infrared spectroscopy (FTIR), Fourier transform Raman spectroscopy (FT-Raman), and NMR to confirm the grafting. For the analysis of the structural information and functional groups of the grafted copolymers, spectral characterizations were made in the range of 400-4000 cm^{-1} using A Nicolet iS10 Fourier model transform infrared spectrometer and FT-Raman module of the same device. Solid state 1H NMR analysis of the powder sample (Route 9) was performed using the Varian Inova Nuclear Magnetic Resonance device (14 kHz 11 Tesla, 500 MHz).

*Published by International Journal of Hydrogen Energy, doi: https://doi.org/10.1016/j.ijhydene.2023.05.345

2.4. Preparation of electrospun mats

The PVDF-*g*-VBC powders are dissolved in DMAc:THF (7:3) solvent mix as the first electrospinning solution. This solution is optimized to the 23 wt.% weight ratio of the grafted polymer to solvent mix for the best fiber structure. For the second electrospinning solution, the same solvent mix of DMAc:THF (7:3) is used with a weight percentage of 15% (total polymer weight to the solution). The polymer mix of the second solution consists of inert PVDF powder and Fumion-FAA-3 in 1:2 and 1:9 ratios. These solutions are drawn as fibers into a rotating drum (300 rpm) as either single fiber form or dual fiber form with 15 kV applied voltage at a 65% humidity level. 9 different mats are prepared in this way with changing the weight ratios of PVDF-*g*-VBC to the total membrane weight as well as 3 different mixes of second solution as listed in Table 2.

Table 2. Polymer and ionomer weight percentages of the solutions for electrospinning and weight percentage of the PVDF-*g*-VBC to the final membrane

Membrane	**First Solution (26 wt%)**	**Second Solution (15 wt%)**	**Weight Percentage of PVDF-*g*-VBC (PVDF-*g*-VBC/Membrane)**
1	PVDF-*g*-VBC (50 kGy)	PVDF:Fumion (1:2)	88%
2	PVDF-*g*-VBC (50 kGy)	PVDF:Fumion (1:2)	78%
3	PVDF-*g*-VBC (50 kGy)	PVDF:Fumion (1:2)	65%
4	PVDF-*g*-VBC (50 kGy)	PVDF	79%
5	PVDF-*g*-VBC (50 kGy)	PVDF:Fumion (1:9)	83%
6	PVDF-*g*-VBC (50 kGy)	-	100%
7	PVDF-*g*-VBC (25 kGy)	-	100%

*Published by International Journal of Hydrogen Energy, doi: https://doi.org/10.1016/j.ijhydene.2023.05.345

8	PVDF-*g*-VBC (25 kGy)	PVDF:Fumion (1:2)	75%
9	PVDF-*g*-VBC (25 kGy)	PVDF	72%

2.5. Characterization of the electrospun mats

Morphologies of the electrospun mats were investigated by using a scanning electron microscope (SEM) (FESEM Gemini Supra 35 VP, LEO model) with an electron voltage of 3 kV and 5000x and 20000x magnifications with a secondary electron detector. Additionally, Energy Dispersive Spectrum (EDS) analysis was performed with an EDS device connected to the SEM-FEG (Zeiss, SUPRA VP 35). The dual-fiber electrospinning of PVDF-*g*-VBC fiber and inert PVDF fibers was analyzed by applying point elemental analysis on the fibers at a working distance of 8.5 mm and applying a voltage of 8 kV.

2.5. Preparation of anion exchange membranes

The prepared electrospun mats were cut into rectangular shapes (8 cm x 5 cm), and hot pressed at 140-160°C for 2.5-10 minutes and 5-10 tons of weight, pressed and then kept in an oven at 90°C for 30 minutes for thermal annealing. The optimized parameters are 150°C, 10 min, and 10 tons for hot-pressing. The hot-pressed films have thicknesses between 40-50 μm. The morphologies of hot-pressed mats were examined with SEM, as described above. The compact membranes are later immersed into trimethylamine (TMA 50%) solution for amination of the VBC grafts. In this way, the chloromethyl groups were converted into quaternary ammonium with fixed charged parts. Then, excess TMA was removed by washing with water. Finally, to replace the Cl^- ions in all the quaternary ammonium parts of the obtained membrane with OH^-, it was left in a 1M KOH solution for 24 hours and then washed with pure water and kept in deionized water until further characterizations were performed. At the end of all these steps, the preparation of the AEMs was completed.

2.6. Characterization of the membranes

The BekkTech conductivity cell was used to measure the conductivity of the electrospun membranes using the Gamry Reference 3000 Potentiostat/Galvanostat system (Gamry Instruments, USA). The resistance values were obtained using 4-probe conductivity measurements with electrochemical impedance spectroscopy. The prepared membranes were cut into dimensions of 2 cm x 2.5 cm and their ionic conductivity was measured at room temperature and 100% humidity. Before measurements, the membranes were soaked in deionized water for at least 4 hours. During the measurements, a constant current of 100 mA was applied through the membranes for 1 hour, as suggested in the study by Ziv et al., to remove carbonate groups formed due to carbon poisoning and to obtain more accurate hydroxide

*Published by International Journal of Hydrogen Energy, doi: https://doi.org/10.1016/j.ijhydene.2023.05.345

conductivity measurements [31]. Ionic conductivity was calculated using the equation provided below [32].

$$\sigma \left[\frac{\text{mS}}{\text{cm}}\right] = \frac{L}{R \times W \times T} \quad (2)$$

Where R is resistance (Ω); T is the thickness of the membrane after hot-pressing (cm); W and L indicate the width of the sample (2 cm) and the distance between the probes (0.425 cm), respectively.

Mohr titration method was used to measure the ion exchange capacity (IEC) of the prepared membranes [33]. 10-30 mg of membranes were cut after the amination step and immersed into the 0.5 M HCl solution was renewed every 12 hours and kept for 24 hours. Then, after washing 3 times with deionized water, the membranes are transferred to 0.2 M $NaNO_3$ solution that is changed every 8 hours, 3 times. These were collected and titrated with 0.01 M $AgNO_3$. In this process, where K_2CrO_4 is used as an indicator, Ag^+ ions in the $AgNO_3$ solution, which is added at a rate of 0.01 ml/s, react with Cl^- to form AgCl molecules. When the color change is achieved thanks to K_2CrO_4, the titration step is completed, and the total used titrant volume is recorded. Then, the dry weights of the titrated membranes were measured after drying at 50°C overnight. With the results of the measurements made, the IEC has been calculated as in the following equation. In this equation, w_{dry} indicates the dry membrane weight and v_{AgNO3} & c_{AgNO3} indicate the volume and molarity of the $AgNO_3$ solution used in the titration.

$$IEC \left[\frac{\text{mmol}}{\text{g}}\right] = \frac{v_{AgNO_3}[\text{ml}] \times c_{AgNO_3}\left[\frac{\text{mmol}}{\text{ml}}\right]}{w_{dry}[\text{g}]} \quad (3)$$

Water uptake of the prepared membranes is also calculated by the weight increase by immersing the membranes in deionized water overnight and measuring the weight of the membranes before and after immersion. The wet measurements were taken after the excess surface water is blotted. The dry measurements were taken after vacuum drying the membranes at 80 °C overnight. The water uptake is calculated as in the following equation.

$$WU\ [\%] = \frac{w_{wet}[\text{g}] - w_{dry}[\text{g}]}{w_{dry}[\text{g}]} \times 100 \quad (4)$$

Where w_{wet} is the weight of the wet membrane, w_{dry} is the weight of the dry membrane.

Tensile tests of the prepared membranes were conducted with the Zwick-Roell Z100 model Universal Testing Machine (UTM). Samples were prepared according to ASTM D882 standards and tested following the standard with fixed crosshead speed at 10 mm/min.

Also, phase properties and mechanical properties were investigated with AFM. AFM-QNM measurements were made with Bruker Multimode 8 AFM with silicon canopy and percussion mode with K=30 N/m (K=spring constant).

*Published by International Journal of Hydrogen Energy, doi:
https://doi.org/10.1016/j.ijhydene.2023.05.345

3. Results and Discussion

3.1. Characterization of PVDF-*g*-VBC powders

The properties of AEMs, prepared with radiation-induced grafting, exhibit significant changes with the degree of grafting [34,35]. As the degree of grafting increases, the density of functional groups on the polymer matrix enhances [34,36]. This results in improved ion conductivity leading to higher overall performance [34,36]. Moreover, increasing the degree of grafting also influences other key properties of the membranes, such as mechanical strength, water uptake etc. [34,36]. By adjusting the degree of grafting, it is possible to fine-tune these properties to meet specific application requirements.

The degrees of grafting, which were calculated using Equation 1 and measured immediately after filtration and drying following the synthesis of the grafted copolymer, are given in Table 1. In the first 4 samples, sufficient grafting could not be observed by the weight difference. It is probably due to the weight change after grafting being less than the loss of weight at the synthesis step. By making individual changes in the reaction parameters, the most optimized state was reached in sample 9. It was observed that especially increasing the N_2 purification time and monomer percentage had significant effects on the degree of grafting. Further confirmation of grafting is done by FTIR, FT-Raman, and NMR analysis.

The results of the FT-Raman analysis of the PVDF-*g*-VBC synthesized with different parameters and the inert PVDF are given in Fig. 3. The peak at 1450 cm^{-1} in the PVDF spectrum indicates the CH_2 scissoring, while the peaks observed at 1001 cm^{-1} and 1611 cm^{-1} resulting from grafting are due to the aromatic structures of VBC attached to PVDF.[30] In addition, the broad peaks between 600 and 800 cm^{-1} belong to the C-Cl bond. The peak at 1266 cm^{-1} indicates successful grafting, which is due to the CH_2Cl degradation [37,38]. As a result of this analysis, it is shown that all the powder samples numbered 7-13 have been successfully grafted.

*Published by International Journal of Hydrogen Energy, doi:
https://doi.org/10.1016/j.ijhydene.2023.05.345

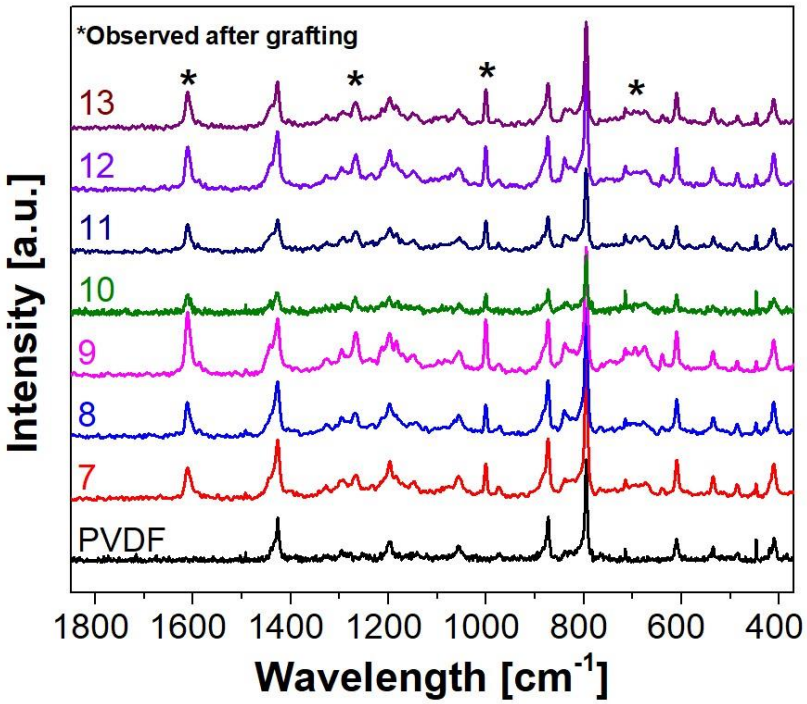

Figure 3. The FT-Raman analysis of PVDF-g-VBC with different parameters and inert PVDF showed peaks indicating characteristic vibrations of PVDF, grafting of VBC aromatic structures, presence of C-Cl bonds, and successful grafting for powder samples 7-13. The peaks that are marked with (*) are emerged after the grafting of VBC onto PVDF

The H-NMR results shown in Fig. 4 also indicate that the grafting process was successfully. The strong peaks observed at 2.5 and 3.4 ppm are respectively due to the DMSO and H_2O peaks of the solvent [39]. The peaks at around 2.9 ppm and 2.2 marked with "a" is seen to be due to the head-tail and head-head arrangement of the PVDF-based polymer in agreement with the literature [40]. In addition, the peak marked with "b" in Fig. 4 is a peak that appears after grafting and comes from the methylene hydrogen in the grafted branch.

*Published by International Journal of Hydrogen Energy, doi:
https://doi.org/10.1016/j.ijhydene.2023.05.345

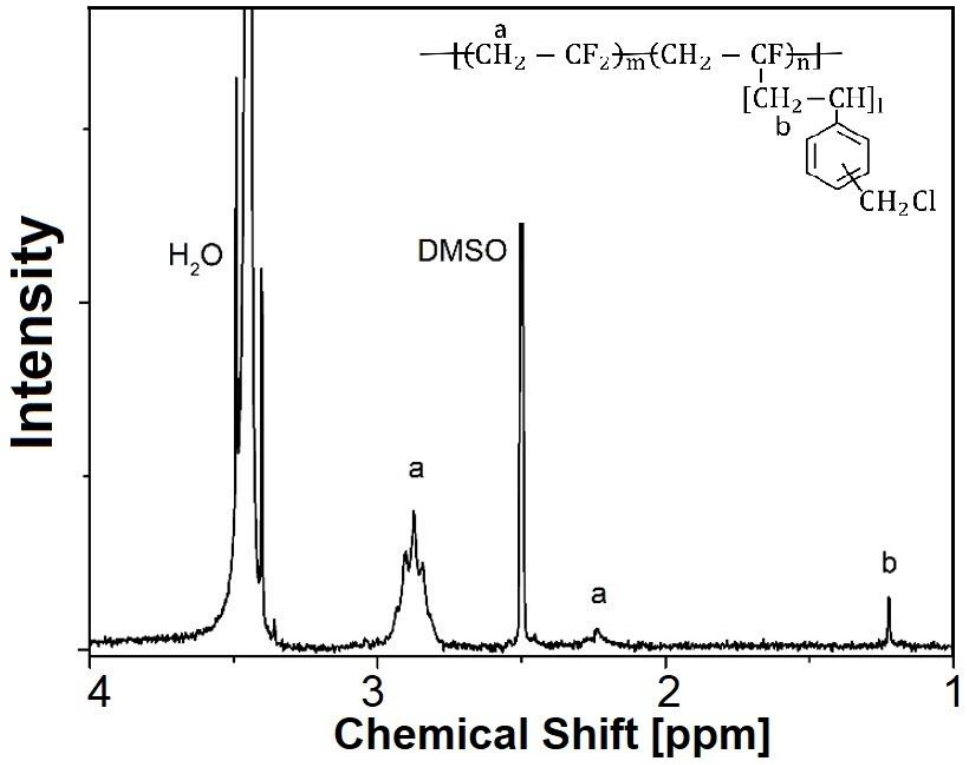

Figure 4. The ^{1}H-NMR spectrum of PVDF-*g*-VBC with an inset of the molecular structure. The peaks are marked with (a) and (b) are corresponding to H atoms that are shown in the inset figure of the molecular structure PVDF-*g*-VBC. The strong peaks at 2.5 and 3.4 ppm are due to solvent and humidity of the sample.

The chemical structures of synthesized copolymers were also investigated by the Fourier transform infrared (FTIR). The FTIR spectra in Fig 5. of PVDF and PVDF-*g*-VBC. The characteristic peaks of PVDF are as expected [41]. The 710 cm^{-1} and 2921 cm^{-1} peaks resulting from the grafting of PVDF correspond to the meta ring position of VBC [42]. This result indicates that the grafting was performed successfully. Additionally, the presence of the major PVDF peaks even after grafting indicates the lack of structural damage due to irradiation. After the amination step, the peaks at 710 cm^{-1} and 2921 cm^{-1} disappeared as seen in the green curve confirming the release of the Cl^{-} while the emergence of the new peaks at 1276 cm^{-1} and 835 cm^{-1} was both due to N-C stretching [43]. These results showed that the amination step was also successful.

*Published by International Journal of Hydrogen Energy, doi:
https://doi.org/10.1016/j.ijhydene.2023.05.345

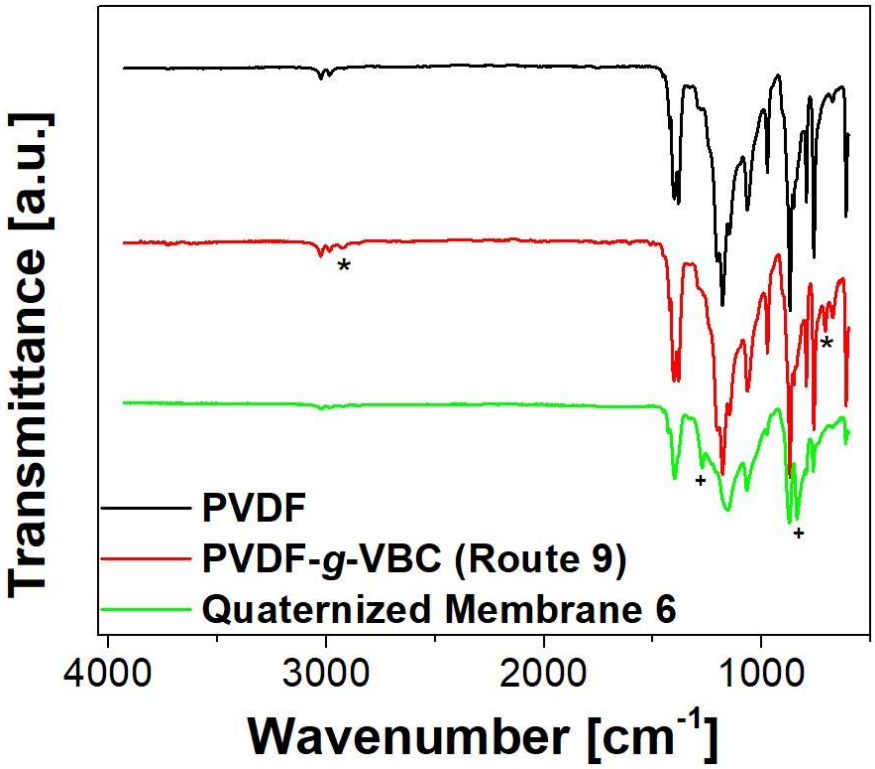

Figure 5. FTIR spectra analysis, revealing characteristic peaks of PVDF, successful grafting indicated by the presence of 710 cm^{-1} and 2921 cm^{-1} peaks corresponding to VBC, lack of structural damage, disappearance of these peaks after amination confirming release of Cl^-, and emergence of new peaks at 1276 cm^{-1} and 835 cm^{-1} indicating successful amination.

3.2. Characterization of the electrospun mats

First, the morphology of the single fiber electrospun of PVDF-*g*-VBC is investigated. The SEM micrograph (5000x) of the mat in Fig. 6a shows a homogeneous distribution of bead-free fibers of PVDF-*g*-VBC fibers. Then fibers of the dual-fiber electrospun mats are investigated. In Fig. 6b SEM micrograph (5000x) of electrospun mats of dual-fiber of PVDF-*g*-VBC and inert PVDF, as well as dual-fiber of PVDF-*g*-VBC and PVDF+Fumion (Fig. 6c) shows homogenous fibers without beads with two different fiber diameters. A Close-up (20000x) micrograph of mats with the PVDF fibers and PVDF-*g*-VBC fibers indicates two distinct surface characteristics. The PVDF-*g*-VBC fibers had a wrinkled surface while PVDF fibers had a more porous surface. These distinguishable fibers were confirmed to be PVDF-*g*-VBC and inert PVDF by the EDS analysis. While both EDS spectra (Fig. 6.e,f) of both fibers had K_α signals of C, and F while the wrinkled fibers had also an additional peak at around 2.6 keV that corresponds to the Cl K_α signal and 0.183 keV signal that corresponds to the Cl L_α [44,45].

*Published by International Journal of Hydrogen Energy, doi: https://doi.org/10.1016/j.ijhydene.2023.05.345

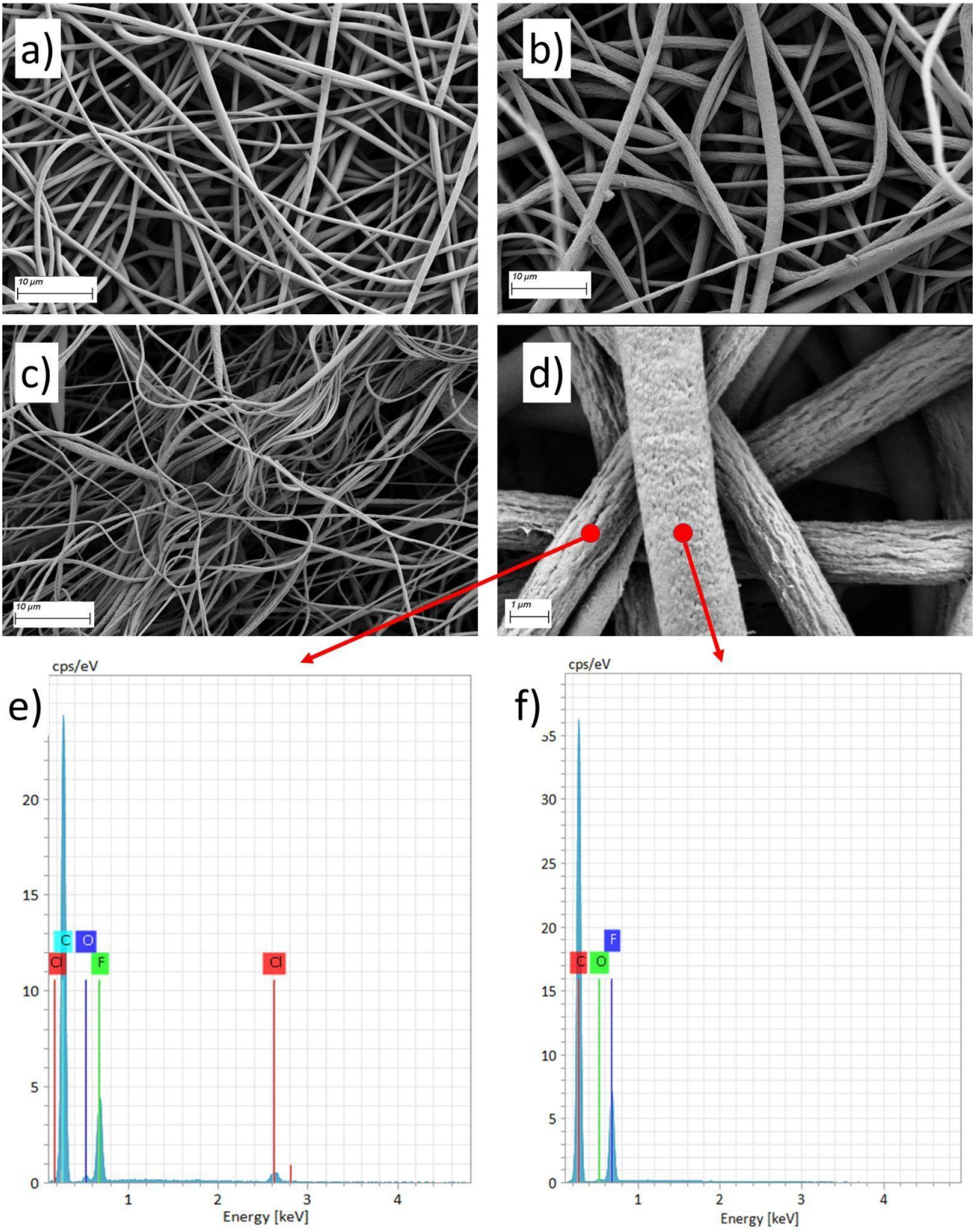

*Published by International Journal of Hydrogen Energy, doi:
https://doi.org/10.1016/j.ijhydene.2023.05.345

Figure 6. SEM micrograph (5000x) of electrospun mats of **a)** single fiber PVDF-*g*-VBC **b)** dual-fiber PVDF-*g*-VBC and PVDF **c)** dual-fiber PVDF-*g*-VBC and PVDF+Fumion **d)** magnified (20000x) micrograph of mats with dual-fiber system of PVDF-*g*-VBC and PVDF **e-f)** energy spectra of the EDS analysis from the pointed spots of the dual-fiber system of PVDF-*g*-VBC and PVDF

After the hot-pressing step, the morphologies of fabricated membranes were investigated with the SEM to check compact structure which would eliminate undesired fuel crossover. The SEM micrograph (5000x) (Fig. 7) of the hot-pressed dual-fiber electrospun mats showed that the mats were compacted without any visible porous structure while keeping the fiber structure intact. Moreover, the mats, that were opaque before the hot-press due to interfiber voids, became transparent which is an indication of the absence of these voids.

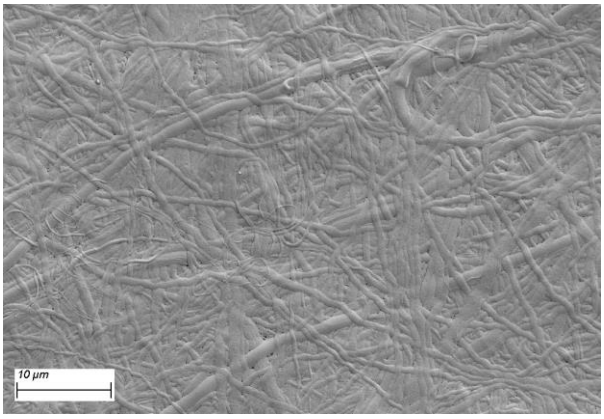

Figure 7. SEM micrograph of hot-pressed dual-fiber electrospun mats

In AFM maps (Fig. 8) of the compacted membranes, it is observed in the peak force error map that a pore-free structure is reached. Additionally, Young's modulus map estimated by the logarithmic Sneddon model fitting analysis provides the regional mechanical properties of the material [43]. It indicates the presence of softer ion exchange channels with low Young's modulus and higher Young's modulus phases surrounding them due to duel fiber structure. The deformation and height maps indicate that the material did not have a porous structure and that the membranes did not show any puncturing during measurement. As a result of the AFM analyses, it has been shown that it is crucial to make dual-fiber electrospinning with a polymer that has a higher mechanical force in order to provide mechanical support to the ion transfer channels. Zhou et al. also similarly showed the ionic conductive channels of their single-fiber electrospun polyketone-based AEMs [46]. However, the microphase separation for the membranes with dual-fibers systems is more definitive.

*Published by International Journal of Hydrogen Energy, doi: https://doi.org/10.1016/j.ijhydene.2023.05.345

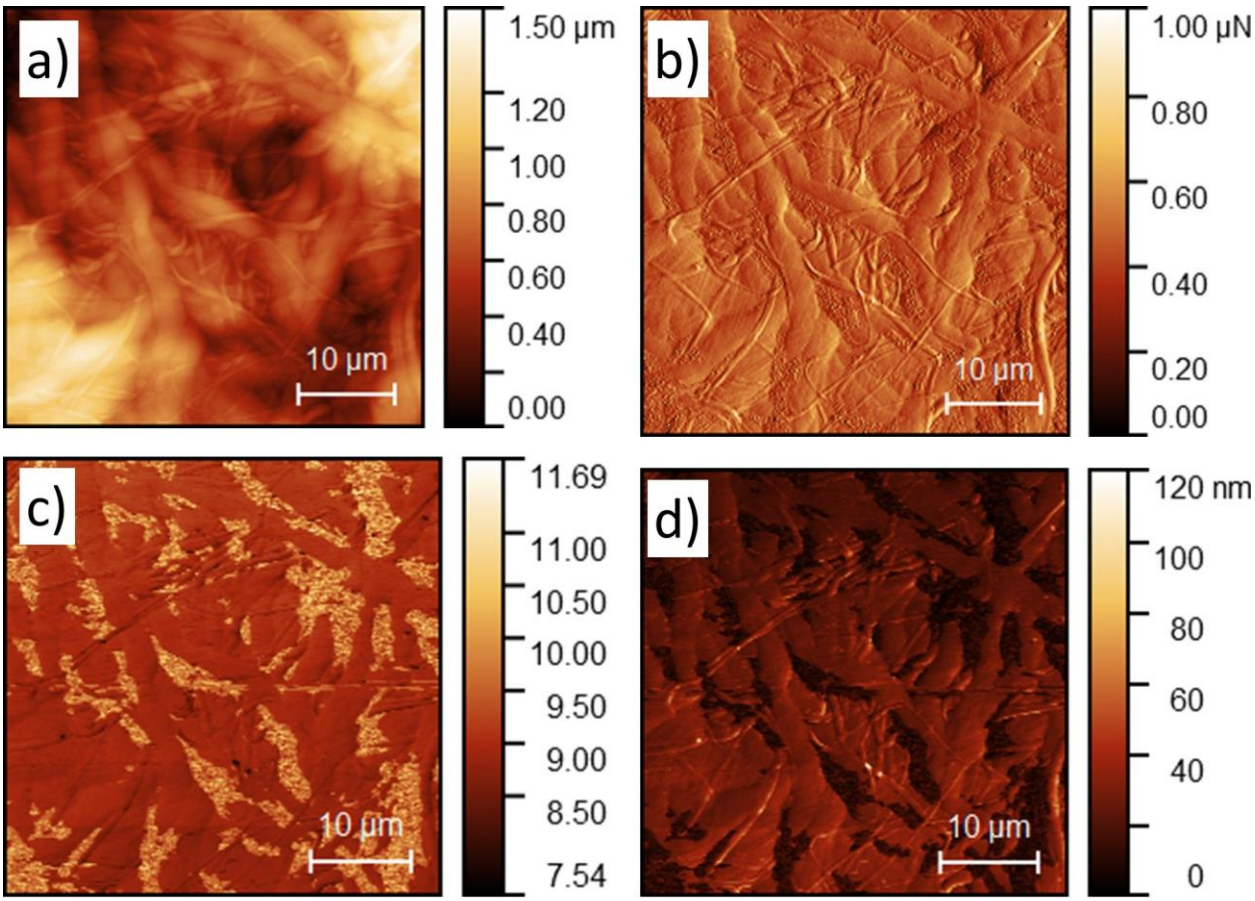

Figure 8. AFM images of the membrane 1 **a)** height map **b)** peak force error map **c)** The Young's modulus map of the membrane estimated by Sneddon model fitting and **d)** the deformation map

The results (Table 3) of the membranes' tensile test after amination showed that strains at breaks between 10-40% and tensile strengths between 10-35 MPa are observed for the membranes produced from powders with 50 kGy irradiation (membranes 1-6). Additionally, Young's modulus results calculated from the slopes in the linear elastic deformation regime range between 760-300 MPa which are in parallel with the reported values of other similar works and commercial membranes [6,47]. The high tensile strain of membrane 4, which reaches up to 40%, can be attributed to the high mechanical properties of PVDF. When examining Young's moduli, the highest stress coefficient is observed in membrane 1. However, when looking at the first three membranes, Young's modulus decreases as the PVDF-*g*-VBC ratio decreases. When comparing the effect of the irradiation dose, it is observed an increase in both tensile strength and Young's modulus for membranes 7-9 prepared with a lower radiated dose (25 kGy). This is expected to be due to higher irradiation doses leading to lower Young's modulus and ultimate tensile strength because of an increase in the C-C bond breakage in the base polymer [6,48]. As a result of these mechanical measurements, it has been observed that the produced membranes are suitable for fuel cell applications in terms of their mechanical properties.

*Published by International Journal of Hydrogen Energy, doi: https://doi.org/10.1016/j.ijhydene.2023.05.345

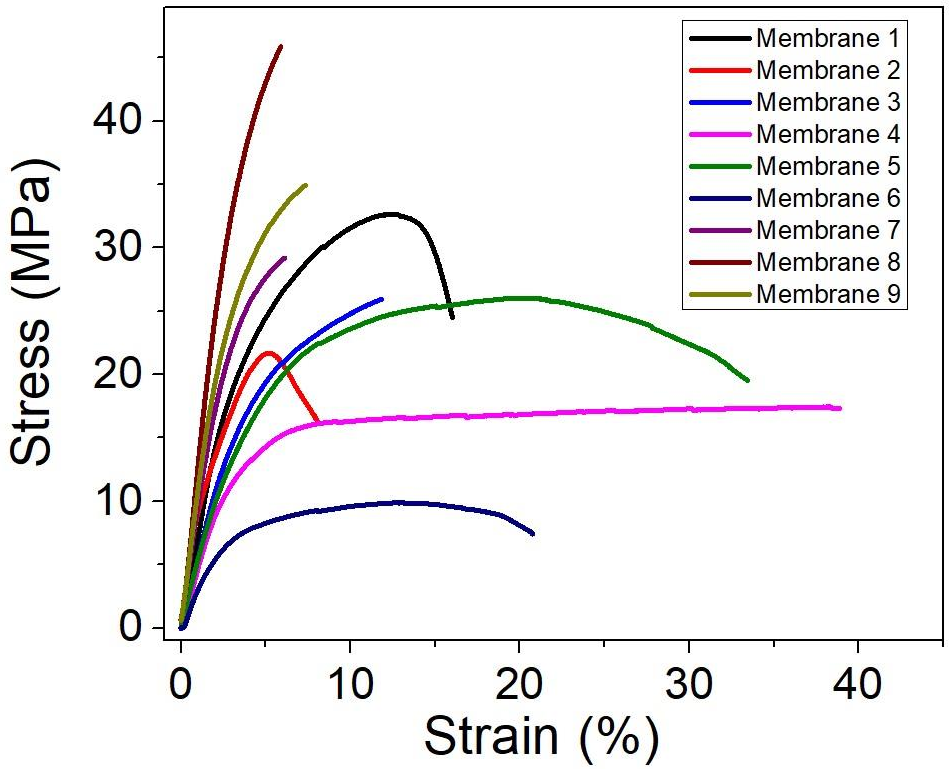

Figure 9. Stress-strain curves of the membranes

The physicochemical properties (IEC and ionic conductivity) of membranes are also investigated in Table 3. Ion exchange capacity is one of the main properties of the AEMs that indicates how much functional group it has per its gram which is important for ionic conductivity mechanisms [40]. When the first 3 membranes are compared to each other, they exhibit close IEC values of 1.2 - 1.3 mmol/g even though the weight percentage of PVDF-*g*-VBC is decreased through membranes 1 to 3. The increase in the Fumion ionomers would balance out the difference. That is also in line with the increase of IEC from membrane 4 (0.8 mmol/g) to membrane 2 (1.17 mmol/g), where the only change is the addition of the commercial ionomer. Comparing single-fiber membrane 6 to membranes 1-3 indicates a slight increase in the IEC values. That would be explained by the addition of Fumion ionomers adding more functional groups when they replace the PVDF-*g*-VBC fibers even with their 1:2 ratio to the inert PVDF. Additionally, the 25 kGy-dosed membranes (membrane 7-9) show almost half of the IEC values of their 50 kGy-dosed counterparts (membrane 2, 4, 6) as expected.

Ionic conductivity mechanisms of the OH^- ions are similar to that of H^+ which generally conducts with hopping mechanisms [49,50]. Having phase-segregated structures that can create conduction channels would lead to higher conductivity levels even with similar IEC values [49,50]. Dual-fiber electrospinning is an ideal technique for both controlling the weight ratios of the ionically active and inert polymers as well as constructing ionic conduction channels with the fiber formation. As mentioned in the AFM section, the dual-fiber membranes have two distinct regions of PVDF+Fumion and PVDF-*g*-VBC. The ionic conductivity of the first 3 membranes is steadily increasing with a direct proportionality to the increase of the weight percentage of PVDF-*g*-VBC

as expected due to having more ionically active channels. Single-fiber structure of the PVDF-*g*-VBC (Membrane 6) has the highest ionic conductivity among the whole membranes too. Addition of the inert PVDF as the second fiber (membrane 4), the conductivity decreases dramatically from that of membrane 6, however, the addition of the ionomers in the second fiber (membrane 5) would increase it back. This can be attributed to the creation of alternative pathways that could lead OH^- conduction from one PVDF-*g*-VBC fiber to another one. An increase in the ionomer ratio between membrane 2 to membrane 5 almost increases it back to the level of single-fiber membrane 6. Similar to the IEC values, ionic conductivity for the lower-dosed (25 kGy) membranes (7-9) are almost an order below their higher-dosed counterparts due to the lower amount of active sites after irradiation.

Water uptake (WU) is also another important factor of the membranes which is generally related to ion exchange capacity and higher water uptake would lead to an increase in ionic conductivity.[18] Even though, the conductivity of OH^- ions requires water molecules for their transport mechanisms, an excessive amount of water also indicates inactive H_2O molecules that are not interacting with the charged parts of the polymer.[43] Additionally, excessive water uptake also decreases the mechanical properties of the membrane due to high swelling.[18,43] When the first three membranes are compared, it can be seen that since IEC levels are similar, their WU's are around the same levels. The addition of the Fumion ionomer to the second solution would explain the increase in the WU from membrane 2 to 4 and comparing the water uptake of membrane 1 and membrane 5 can give us information about changing the Fumion ionomer ratio among the reinforcing fibers. Increasing this ratio from 1:2 to 1:9 is decreasing the water uptake. In addition to this, the fact that the lower-dosed (25 kGy) membranes (7 - 9) have also lower water uptakes than their 50 kGy counterparts can be explained again by the lower amount of active sides due to less irradiation.

Table 3. Physicochemical and mechanical properties of the prepared membranes

Membrane	Conductivity at 25 °C [mS/cm]	Ion Exchange Capacity [mmol/g]	Water Uptake [%]	Young Modulus [MPa]	Stress at break [MPa]	Strain at break [%]
1	4.67	1.35	11.7	761	24.4	16.0
2	1.77	1.17	12.2	458	16.1	8.1
3	1.42	1.22	10.7	436	25.9	11.8
4	0.71	0.80	9.3	360	17.3	38.8
5	5.08	0.80	5.6	320	19.5	33.4

*Published by International Journal of Hydrogen Energy, doi: https://doi.org/10.1016/j.ijhydene.2023.05.345

6	5.53	1.03	18.1	299	7.4	20.7
7	0.27	0.65	5.8	734	29.0	6.0
8	0.3	0.62	6.0	1119	45.8	5.8
9	0.24	0.42	5.3	819	34.7	7.1

4. Conclusions

In summary, the synthesis of AEMs based on PVDF-*g*-VBC by radiation-induced grafting followed by dual-fiber electrospinning methods was successfully achieved through a broad optimization study. The grafting reaction was confirmed by chemical analyses with FTIR, FT-Raman, and NMR and the degrees of grafting were measured by the weight increase. Subsequently, the synthesized graft copolymers were used together with inert PVDF powders and Fumion-FAA-3 ionomers in various ratios to produce nine different mats via dual-fiber electrospinning. These mats were then converted into compact films by hot pressing. These films were aminated and subjected to ion exchange and were extensively examined in terms of mechanical, ionic, and morphological properties. Particularly promising results in terms of low water uptake, high ion exchange capacity, and high mechanical strength were obtained in hybrid membranes produced using the radiation-grafted PVDF-*g*-VBC membranes by dual-fiber electrospinning for the first time in the literature for the production of AEM. Comparative analyses of each membrane pair showed a promising way to control the physicochemical and mechanical properties of the AEM membranes. The membrane 1 which was prepared with PVDF-*g*-VBC (88 wt.%), with PVDF:Fumion-FAA-3 (1:2, 12 wt.%) mix showed an OH^- conductivity of 4.67 mS/cm at 25 ^oC, with ion exchange capacity of 1.35 mmol/g with Young's Modulus of 761 MPa. In conclusion, the combination of dual-fiber electrospinning with radiation-grafting would create membrane structures tunable in terms of their physicochemical and mechanical properties. For future direction, the scope of this work can be extended by employing various other head groups, polymer backbone, and grafting monomers to develop better membranes for the anion exchange membrane fuel cells.

*Published by International Journal of Hydrogen Energy, doi:
https://doi.org/10.1016/j.ijhydene.2023.05.345

Acknowledgements

The authors gratefully acknowledge the financial support of The Scientific and Technological Research Council of Turkey (TÜBİTAK) (Grant Number: 119M059)

The authors thank Bilal Iskandarani for his assistance in experiments.

Conflicts of interest

There are no conflicts to declare.

Abbreviations

AEMFC: Anion Exchange Membrane Fuel Cells

AEM: Anion Exchange Membrane

AFM: Atomic Force Microscopy

CMPSF: Chloromethylated polysulfone

EDS: Energy Dispersive Spectrum

FTIR: Fourier Transform Infrared Spectroscopy

FT-Raman: Fourier Transform Raman

NMR: Nuclear Magnetic Resonance

PEMFC: Proton Exchange Membrane Fuel Cells

PGM: Platinum Group Metals

PPSU: polyphenylsulfone

*Published by International Journal of Hydrogen Energy, doi: https://doi.org/10.1016/j.ijhydene.2023.05.345

PVDF: poly(vinylidenefluoride)

PVDF-g-VBC: Poly(vinylidene fluoride) Grafted with Vinylbenzyl Chloride

SEM: Scanning Electron Microscope

UTM: Universal Testing Machine

VBC: Vinylbenzyl chloride

References

[1] Perera F. Pollution from fossil-fuel combustion is the leading environmental threat to global pediatric health and equity: Solutions exist. Int J Environ Res Public Health 2018;15. https://doi.org/10.3390/ijerph15010016.

[2] Das G, Choi JH, Nguyen PKT, Kim DJ, Yoon YS. Anion Exchange Membranes for Fuel Cell Application: A Review. Polymers (Basel) 2022;14. https://doi.org/10.3390/polym14061197.

[3] Wu G, More KL, Johnston CM, Zelenay P. High-performance electrocatalysts for oxygen reduction derived from polyaniline, iron, and cobalt. Science (1979) 2011;332:443–7. https://doi.org/10.1126/science.1200832.

[4] Mamlouk M, Wang X, Scott K, Horsfall JA, Williams C. Characterization and application of anion exchange polymer membranes with non-platinum group metals for fuel cells. Proceedings of the Institution of Mechanical Engineers, Part A: Journal of Power and Energy 2011;225:152–60. https://doi.org/10.1177/2041296710394264.

[5] Bezerra CWB, Zhang L, Lee K, Liu H, Marques ALB, Marques EP, et al. A review of Fe-N/C and Co-N/C catalysts for the oxygen reduction reaction. Electrochim Acta 2008;53:4937–51. https://doi.org/10.1016/j.electacta.2008.02.012.

[6] Wang L, Magliocca E, Cunningham EL, Mustain WE, Poynton SD, Escudero-Cid R, et al. An optimised synthesis of high performance radiation-grafted anion-exchange membranes. Green Chemistry 2017;19:831–43. https://doi.org/10.1039/C6GC02526A.

[7] Vijayakumar V, Nam SY. A Review of Recent Chitosan Anion Exchange Membranes for Polymer Electrolyte Membrane Fuel Cells. Membranes (Basel) 2022;12:1–12. https://doi.org/10.3390/membranes12121265.

[8] Cheng J, He G, Zhang F. A mini-review on anion exchange membranes for fuel cell applications: Stability issue and addressing strategies. Int J Hydrogen Energy 2015;40:7348–60. https://doi.org/10.1016/j.ijhydene.2015.04.040.

[9] Yokota N, Ono H, Miyake J, Nishino E, Asazawa K, Watanabe M, et al. Anion conductive aromatic block copolymers containing diphenyl ether or sulfide groups

*Published by International Journal of Hydrogen Energy, doi: https://doi.org/10.1016/j.ijhydene.2023.05.345

for application to alkaline fuel cells. ACS Appl Mater Interfaces 2014;6:17044–52. https://doi.org/10.1021/am5046586.
[10] Zhang F, Zhang H, Qu C. Influence of solvent on polymer prequaternization toward anion-conductive membrane fabrication for all-vanadium flow battery. Journal of Physical Chemistry B 2012;116:9016–22. https://doi.org/10.1021/jp304880r.
[11] Varcoe JR, Slade RCT. An electron-beam-grafted ETFE alkaline anion-exchange membrane in metal-cation-free solid-state alkaline fuel cells. Electrochem Commun 2006;8:839–43. https://doi.org/10.1016/j.elecom.2006.03.027.
[12] Ponce-González J, Whelligan DK, Wang L, Bance-Soualhi R, Wang Y, Peng Y, et al. High performance aliphatic-heterocyclic benzyl-quaternary ammonium radiation-grafted anion-exchange membranes. Energy Environ Sci 2016;9:3724–35. https://doi.org/10.1039/c6ee01958g.
[13] Li Y, Xu T, Gong M. Fundamental studies of a new series of anion exchange membranes: Membranes prepared from bromomethylated poly(2,6-dimethyl-1,4-phenylene oxide) (BPPO) and pyridine. J Memb Sci 2006;279:200–8. https://doi.org/10.1016/j.memsci.2005.12.006.
[14] Wang L, Peng X, Mustain WE, Varcoe JR. Radiation-grafted anion-exchange membranes: the switch from low-to high-density polyethylene leads to remarkably enhanced fuel cell performance †. Energy Environ Sci 2019;12:1575. https://doi.org/10.15126/surreydata.8050274.
[15] Li L, Deng B, Ji Y, Yu Y, Xie L, Li J, et al. A novel approach to prepare proton exchange membranes from fluoropolymer powder by pre-irradiation induced graft polymerization. J Memb Sci 2010;346:113–20. https://doi.org/10.1016/j.memsci.2009.09.027.
[16] Sherazi TA, Ahmad S, Kashmiri MA, Guiver MD. Radiation-induced grafting of styrene onto ultra-high molecular weight polyethylene powder and subsequent film fabrication for application as polymer electrolyte membranes: I. Influence of grafting conditions. J Memb Sci 2008;325:964–72. https://doi.org/10.1016/j.memsci.2008.09.028.
[17] Poynton SD, Slade RCT, Omasta TJ, Mustain WE, Escudero-Cid R, Ocón P, et al. Preparation of radiation-grafted powders for use as anion exchange ionomers in alkaline polymer electrolyte fuel cells. J Mater Chem A Mater 2014;2:5124–30. https://doi.org/10.1039/c4ta00558a.
[18] Ballengee JB, Pintauro PN. Composite fuel cell membranes from dual-nanofiber electrospun mats. Macromolecules 2011;44:7307–14. https://doi.org/10.1021/ma201684j.
[19] Zhu L, Pan J, Wang Y, Han J, Zhuang L, Hickner MA. Multication Side Chain Anion Exchange Membranes. Macromolecules 2016;49:815–24. https://doi.org/10.1021/acs.macromol.5b02671.
[20] Sherazi TA, Zahoor S, Raza R, Shaikh AJ, Naqvi SAR, Abbas G, et al. Guanidine functionalized radiation induced grafted anion-exchange membranes for solid alkaline fuel cells. Int J Hydrogen Energy 2015;40:786–96. https://doi.org/10.1016/j.ijhydene.2014.08.086.

*Published by International Journal of Hydrogen Energy, doi: https://doi.org/10.1016/j.ijhydene.2023.05.345

[21] Tamura T, Kawakami H. Aligned electrospun nanofiber composite membranes for fuel cell electrolytes. Nano Lett 2010;10:1324–8. https://doi.org/10.1021/nl1007079.
[22] Sood R, Cavaliere S, Jones DJ, Rozière J. Electrospun nanofibre composite polymer electrolyte fuel cell and electrolysis membranes. Nano Energy 2016;26:729–45. https://doi.org/10.1016/j.nanoen.2016.06.027.
[23] Choi J, Lee KM, Wycisk R, Pintauro PN, Mather PT. Nanofiber composite membranes with low equivalent weight perfluorosulfonic acid polymers. J Mater Chem 2010;20:6282–90. https://doi.org/10.1039/c0jm00441c.
[24] Li HY, Liu YL. Polyelectrolyte composite membranes of polybenzimidazole and crosslinked polybenzimidazole-polybenzoxazine electrospun nanofibers for proton exchange membrane fuel cells. J Mater Chem A Mater 2013;1:1171–8. https://doi.org/10.1039/c2ta00270a.
[25] Wycisk R, Pintauro PN, Park JW. New developments in proton conducting membranes for fuel cells. Curr Opin Chem Eng 2014;4:71–8. https://doi.org/10.1016/j.coche.2014.01.012.
[26] Shang Z, Wycisk R, Pintauro P. Electrospun Composite Proton-Exchange and Anion-Exchange Membranes for Fuel Cells. Energies (Basel) 2021;14:6709. https://doi.org/10.3390/en14206709.
[27] Park AM, Pintauro PN. Alkaline Fuel Cell Membranes from Electrospun Fiber Mats. Electrochemical and Solid-State Letters 2012;15:B27. https://doi.org/10.1149/2.010203esl.
[28] Park AM, Turley FE, Wycisk RJ, Pintauro PN. Electrospun and cross-linked nanofiber composite anion exchange membranes. Macromolecules 2014;47:227–35. https://doi.org/10.1021/ma401932h.
[29] Park AM, Pintauro PN. Alkaline fuel cell membranes from electrospun fiber mats. Electrochemical and Solid-State Letters 2012;15. https://doi.org/10.1149/2.010203esl.
[30] Park AM, Turley FE, Wycisk R, Pintauro PN. Polysulfone-Based Electrospun Anion Exchange Membranes. ECS Meeting Abstracts 2013;MA2013-02:1312–1312. https://doi.org/10.1149/ma2013-02/15/1312.
[31] Ziv N, Dekel DR. A practical method for measuring the true hydroxide conductivity of anion exchange membranes. Electrochem Commun 2018;88:109–13. https://doi.org/10.1016/j.elecom.2018.01.021.
[32] Germer W, Harms C, Tullius V, Leppin J, Dyck A. Comparison of conductivity measurement systems using the example of nafion and anion exchange membrane. Solid State Ion 2015;275:71–4. https://doi.org/10.1016/j.ssi.2015.02.023.
[33] Yan J, Hickner MA. Anion exchange membranes by bromination of benzylmethyl-containing poly(sulfone)s. Macromolecules 2010;43:2349–56. https://doi.org/10.1021/ma902430y.
[34] Fang J, Yang Y, Lu X, Ye M, Li W, Zhang Y. Cross-linked, ETFE-derived and radiation grafted membranes for anion exchange membrane fuel cell applications.

*Published by International Journal of Hydrogen Energy, doi: https://doi.org/10.1016/j.ijhydene.2023.05.345

Int J Hydrogen Energy 2012;37:594–602. https://doi.org/10.1016/j.ijhydene.2011.09.112.
[35] Danks TN, Slade RCT, Varcoe JR. Alkaline anion-exchange radiation-grafted membranes for possible electrochemical application in fuel cells. J Mater Chem 2003;13:712–21. https://doi.org/10.1039/b212164f.
[36] Alkan Gürsel S, Gubler L. Radiation Grafted Membranes. In: Scherer GG, editor. Fuel Cells I, Berlin, Heidelberg: Springer Berlin Heidelberg; 2008, p. 157–217. https://doi.org/10.1007/12_2008_153.
[37] Umar Y, Abdalla S. Experimental FTIR and Theoretical Investigation of the Molecular Structure and Vibrational Spectra of Terephthaloyl Chloride by Density Functional Theory. IOSR Journal of Applied Chemistry I 2015;8:26–34. https://doi.org/10.9790/5736-08912634.
[38] Danks TN, Slade RCT, Varcoe JR. Alkaline anion-exchange radiation-grafted membranes for possible electrochemical application in fuel cells. J Mater Chem 2003;13:712–21. https://doi.org/10.1039/b212164f.
[39] Ran J, Wu L, Lin X, Jiang L, Xu T. Synthesis of soluble copolymers bearing ionic graft for alkaline anion exchange membrane. RSC Adv 2012;2:4250–7. https://doi.org/10.1039/c2ra20336g.
[40] Xia W, Zhang Z. PVDF-based dielectric polymers and their applications in electronic materials. IET Nanodielectrics 2018;1:17–31. https://doi.org/10.1049/iet-nde.2018.0001.
[41] Dong H, Xiao K, Tang X, Zhang Z, Dai J, Long R, et al. Preparation and characterization of polyurethane (PU)/polyvinylidene fluoride (PVDF) blending membrane. Desalination Water Treat 2016;57:3405–13. https://doi.org/10.1080/19443994.2014.988659.
[42] Espiritu R, Mamlouk M, Scott K. Study on the effect of the degree of grafting on the performance of polyethylene-based anion exchange membrane for fuel cell application. Int J Hydrogen Energy 2016;41:1120–33. https://doi.org/10.1016/j.ijhydene.2015.10.108.
[43] Zou M, Liao C, Liu S, Xiong C, Zhao C, Zhao J, et al. Fiber-tip polymer clamped-beam probe for high-sensitivity nanoforce measurements. Light Sci Appl 2021;10. https://doi.org/10.1038/s41377-021-00611-9.
[44] Kritcher AL, Neumayer P, Urry MK, Robey H, Niemann C, Landen OL, et al. K-alpha conversion efficiency measurements for X-ray scattering in inertial confinement fusion plasmas. High Energy Density Phys 2007;3:156–62. https://doi.org/10.1016/j.hedp.2007.02.012.
[45] BRUKER. Periodic Table of Elements and X-ray Energies. n.d.
[46] Zhou YC, Bao RY, Liu Z, Yang MB, Yang W. Electrospun Modified Polyketone-Based Anion Exchange Membranes with High Ionic Conductivity and Robust Mechanical Properties. ACS Appl Energy Mater 2021;4:5187–200. https://doi.org/10.1021/acsaem.1c00727.
[47] Vandiver MA, Caire BR, Carver JR, Waldrop K, Hibbs MR, Varcoe JR, et al. Mechanical Characterization of Anion Exchange Membranes by Extensional

Rheology under Controlled Hydration. J Electrochem Soc 2014;161:H677–83. https://doi.org/10.1149/2.0971410jes.
[48] Yarar Kaplan B, Kirlioğlu AC, Jamil E, Yürüm A, Rajabalizadeh N, Haghmoradi N, et al. Radiation-Grafted Polymer Electrolyte Membranes for Fuel Cells. Hacettepe Journal of Biology and Chemistry 2020;48:483–506. https://doi.org/10.15671/hjbc.813239.
[49] Varcoe JR, Atanassov P, Dekel DR, Herring AM, Hickner MA, Kohl PA, et al. Anion-exchange membranes in electrochemical energy systems. Energy Environ Sci 2014;7:3135–91. https://doi.org/10.1039/c4ee01303d.
[50] Tuckerman ME, Marx D, Parrinello M. The nature and transport mechanism of hydrated hydroxide ions in aqueous solution. Nature 2002;417:925–9. https://doi.org/10.1038/nature00797.

*Published by International Journal of Hydrogen Energy, doi: https://doi.org/10.1016/j.ijhydene.2023.05.345